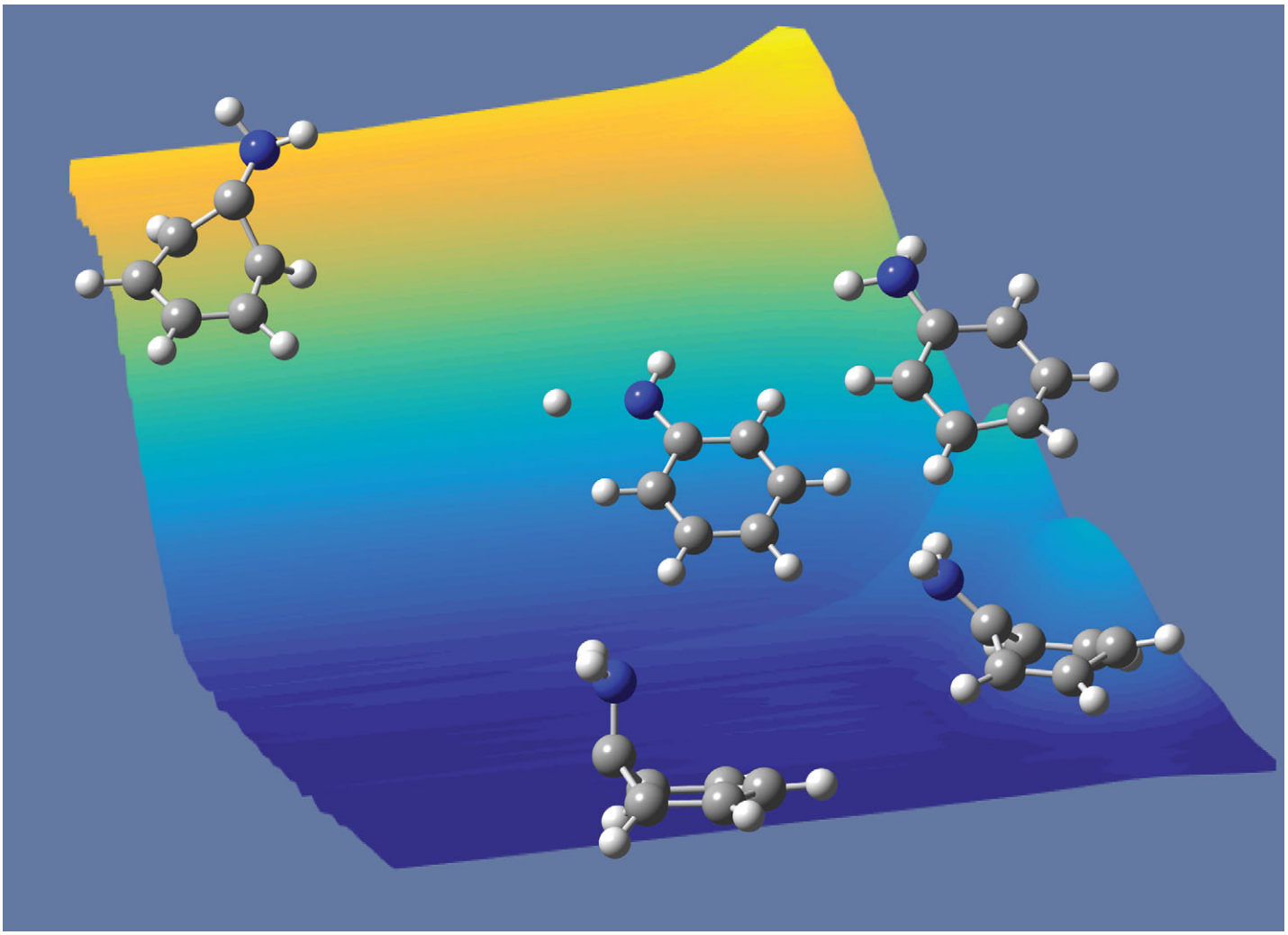

Showcasing research from the group of Prof. Helen Fielding from the Department of Chemistry at University College London.

Title: Comparing the electronic relaxation dynamics of aniline and d_7-aniline following excitation at 272–238 nm

This paper reports femtosecond time-resolved photoelectron spectroscopy experiments comparing the electronic relaxation dynamics of aniline and d_7-aniline. It is found that tunnelling does not play a role in the electronic relaxation dynamics and the authors present what they believe is the first report of the experimental signature of a 3-state conical intersection.

As featured in:

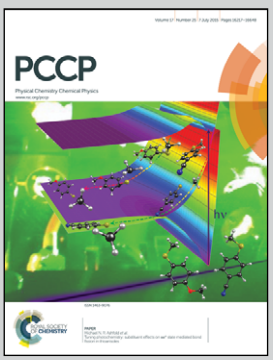

See Helen H. Fielding *et al.*, *Phys. Chem. Chem. Phys.*, 2015, **17**, 16270.

ROYAL SOCIETY OF CHEMISTRY

www.rsc.org/pccp

Registered charity number: 207890

PCCP

PAPER

View Article Online
View Journal | View Issue

Cite this: *Phys. Chem. Chem. Phys.*, 2015, **17**, 16270

Comparing the electronic relaxation dynamics of aniline and d_7-aniline following excitation at 272–238 nm†

Oliver M. Kirkby,[a] Matthieu Sala,[b] Garikoitz Balerdi,[c] Rebeca de Nalda,[d] Luis Bañares,[c] Stéphane Guérin[b] and Helen H. Fielding*[a]

Received 31st March 2015,
Accepted 13th May 2015

DOI: 10.1039/c5cp01883h

www.rsc.org/pccp

Femtosecond time-resolved photoelectron spectroscopy experiments have been used to compare the electronic relaxation dynamics of aniline and d_7-aniline following photoexcitation in the range 272–238 nm. Together with the results of recent theoretical investigations of the potential energy landscape [M. Sala, O. M. Kirkby, S. Guérin and H. H. Fielding, *Phys. Chem. Chem. Phys.*, 2014, **16**, 3122], these experiments allow us to resolve a number of unanswered questions surrounding the nonradiative relaxation mechanism. We find that tunnelling does not play a role in the electronic relaxation dynamics, which is surprising given that tunnelling plays an important role in the electronic relaxation of isoelectronic phenol and in pyrrole. We confirm the existence of two time constants associated with dynamics on the $1^1\pi\sigma^*$ surface that we attribute to relaxation through a conical intersection between the $1^1\pi\sigma^*$ and $1^1\pi\pi^*$ states and motion on the $1^1\pi\sigma^*$ surface. We also present what we believe is the first report of an experimental signature of a 3-state conical intersection involving the $2^1\pi\pi^*$, $1^1\pi\sigma^*$ and $1^1\pi\pi^*$ states.

1 Introduction

There is continuing interest in the role of $^1\pi\sigma^*$ states in the photochemistry of small aromatic molecules containing OH and NH groups.[1,2] These states are characterised by dissociative potential energy curves along O–H or N–H stretching coordinates and have been shown to provide efficient electronic relaxation pathways to conical intersections with the electronic ground state. Consequently, these dissociative states play an important role in protecting biological molecules from harmful photochemical reactions.[3–5]

Aniline ($C_6H_5NH_2$) is a structural motif found in the purine nucleotides, adenine and guanine, and in the pyrimidine nucleotide, cytosine. The UV absorption spectrum of aniline is dominated by two bands centered around 282 nm and 230 nm, corresponding to $\pi^* \leftarrow \pi$ transitions to the first two $^1\pi\pi^*$ states, labelled $1^1\pi\pi^*$ and $2^1\pi\pi^*$ (Fig. 1).[6–11] The first $^1\pi\sigma^*$ state, labelled $1^1\pi\sigma^*$, lies between the $1^1\pi\pi^*$ and $2^1\pi\pi^*$ states.[7] It is composed of N-centered π3s and $\pi\sigma^*$ configurations, arising from $3s \leftarrow \pi$ and $\sigma^* \leftarrow \pi$ transitions, respectively.[12,13] The $1^1\pi\sigma^*$ state has π3s character in the Franck–Condon region but becomes dissociative along the N–H stretch coordinate and forms conical intersections with the $1^1\pi\pi^*$ state and ground electronic state at modest N–H bond-lengths. It has also been proposed that the two 3p Rydberg states may lie between the $1^1\pi\pi^*$ and $2^1\pi\pi^*$ states.[14,15]

There have been a number of recent experimental studies of the photochemistry and photophysics of isolated aniline molecules *in vacuo* using H-atom (Rydberg) photofragment translational spectroscopy,[16] femtosecond pump–probe photoionisation spectroscopy,[17] femtosecond pump–probe velocity map imaging,[18] and time-resolved photoelectron imaging spectroscopy.[19–22] There have also been a number of recent theoretical investigations of the potential energy landscape and relaxation pathways following photoexcitation to the first few singlet excited states.[14,18,23] However, there is not yet a consensus on the electronic relaxation mechanism.

Questions that remain are: (1) Is there evidence to support the suggestion that following excitation close to the $1^1\pi\sigma^*$ origin, tunnelling occurs through the barrier on the $1^1\pi\sigma^*$ potential surface?[16,18,21] (2) Following excitation above the $1^1\pi\sigma^*$ origin, is the relaxation pathway $1^1\pi\sigma^* \rightarrow 1^1\pi\pi^*$[19,20] or $1^1\pi\pi^* \rightarrow 1^1\pi\sigma^*$?[16–18] (3) Is there evidence to support the

[a] Department of Chemistry, University College London, 20 Gordon Street, London WC1H 0AJ, UK. E-mail: h.h.fielding@ucl.ac.uk
[b] Laboratoire Interdisciplinaire Carnot de Bourgogne UMR 6303 CNRS, Université Bourgogne Franche-Comté, 9 Av. A. Savary, BP 47870, F-21078 Dijon Cedex, France
[c] Departamento de Química Física I (Unidad Asociada I + D + i al CSIC), Facultad de Ciencias Químicas, Universidad Complutense de Madrid, 28040 Madrid, Spain
[d] Instituto de Química Física Rocasolano, CSIC, C/Serrano 119, 28006 Madrid, Spain

† Electronic supplementary information (ESI) available: Time constant fits and decay associated spectra residuals. See DOI: 10.1039/c5cp01883h

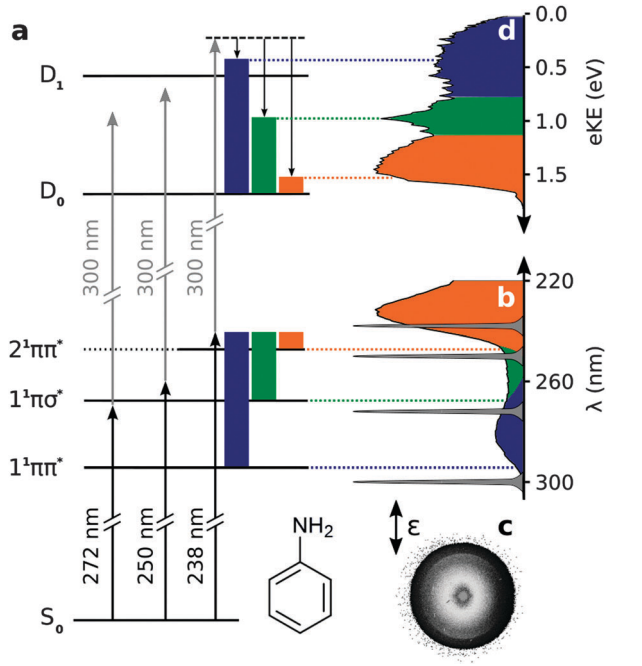

Fig. 1 (a) Schematic excitation scheme in aniline. Solid coloured blocks represent vibrational energy in the excited electronic states of aniline and the equivalent vibrational energy in the ground electronic state of the cation, illustrating the propensity for $\Delta v = 0$ upon photoionisation. (b) Gas-phase absorption spectrum of aniline and spectral profiles of pump and probe laser pulses. Representative photoelectron image (c) and spectrum (d) of aniline collected with pump–probe delay $t = -13$ fs, using a 238 nm pump and 300 nm probe. The double-headed arrow shows the direction of the electric field vector of the pump and probe photons.

suggestion that non-radiative decay from the $2^1\pi\pi^*$ state to the ground-state passes through a three-state conical intersection involving the $2^1\pi\pi^*$, $1^1\pi\sigma^*$ and $1^1\pi\pi^*$ states[23] or a $2^1\pi\pi^*/1^1\pi\pi^*$ conical intersection[18] or involves the 3p Rydberg states?[14]

These questions motivated us to revisit the nonradiative relaxation dynamics of aniline and, in this paper, we present the results of new femtosecond time-resolved photoelectron spectroscopy experiments comparing the relaxation dynamics of aniline and deuterated aniline (d_7-aniline) following photoexcitation in the range 272–238 nm, from just below the $1^1\pi\sigma^*$ origin up to the $2^1\pi\pi^*$ state.

2 Methods

The experimental setup has been described elsewhere.[19,20,24–26] Briefly, aniline (Sigma-Aldrich, >99%) and d_7-aniline (98%, Sigma-Aldrich) were introduced into the velocity map imaging spectrometer by passing 800 mbar helium carrier gas through the liquid samples and expanding through a 50 μm nozzle. After collimation by a 1 mm skimmer, the molecular beam was intersected by femtosecond pump (272–238 nm) and probe (300 nm) laser pulses generated by frequency upconverting the outputs of two optical parametric amplifiers pumped by a commercial amplified Ti:sapphire femtosecond laser system. Pump–probe cross-correlation full-width half-maximum (FWHM) measurements were in the range 180–225 fs. The pump and probe fluxes were attenuated to ~1 μJ per pulse to minimise multiphoton processes and to keep the photoelectron count-rates below 20 photoelectrons per pulse, thus avoiding space-charge effects. The probe wavelength was selected to access as much of the ionisation continuum as possible whilst keeping $1^1\pi\pi^* \leftarrow S_0$ absorption to a minimum (Fig. 1). Multiphoton ionisation time-of-flight mass spectra were recorded to ensure minimal cluster formation and fragmentation of the parent molecules before collecting photoelectron images.

For each excitation wavelength, a set of approximately 18 photoelectron images with pump–probe delays in the range −0.2 ps to 1 ps were recorded, together with the total integrated photoelectron signal for pump–probe delays from −0.5 ps to 100 ps (272 nm) and −0.5 ps to 10 ps (250 nm and 238 nm). Photoelectron velocity distributions were recovered from the raw photoelectron images using the pBasex image inversion algorithm[27] and the energy scale was calibrated by recording the 2 + 1 resonance-enhanced multiphoton ionisation spectrum of Xe at 249.6 nm.[28] The resolution was ~3.5%.

To extract decay times from a set of time-resolved photoelectron spectra, the total integrated areas of the photoelectron spectra recorded at each pump–probe delay were scaled to the total integrated photoelectron signal intensity and then integrated portions of the set of spectra were fit to sums of exponentially decaying profiles convoluted with a Gaussian cross-correlation function representing the cross-correlation of the pump and probe laser pulses $g(t)$,[19,20]

$$S(t) = \sum_i c_i e^{-t/\tau_i} \otimes g(t). \quad (1)$$

c_i is the intensity of the ith decay with $1/e$ decay time τ_i.

Compared with our previous work,[19,20] our data analysis software has been rewritten and is now based on a least-squares fit using the Levenberg–Marquardt optimisation algorithm. We also increased the number of images collected for pump–probe delays between ±100 fs to improve confidence in our determination of $t = 0$ and the cross-correlation from our fitting procedure.

3 Results

Fig. 1(d) shows a representative photoelectron spectrum recorded at −13 fs pump–probe delay following photoexcitation at 238 nm in aniline. The propensity for vibrational energy to be conserved during photoionisation allows us to assign the asymmetric feature at high eKE to ionisation from the $2^1\pi\pi^*$ state and the symmetric feature at low eKE to ionisation from the $1^1\pi\pi^*$ state (Fig. 1).[19,20] This $\Delta v = 0$ propensity also allows us to assign the narrow peak at 1 eV to ionisation from the $1^1\pi\sigma^*$ state and its anisotropic photoelectron angular distribution (maximum $\beta \approx 0.8$) is consistent with ionisation from a π3s configuration.

Time-resolved photoelecron spectra are shown in Fig. 2. We do not observe any variation in anisotropy parameter with pump–probe delay for aniline or d_7-aniline, in agreement with

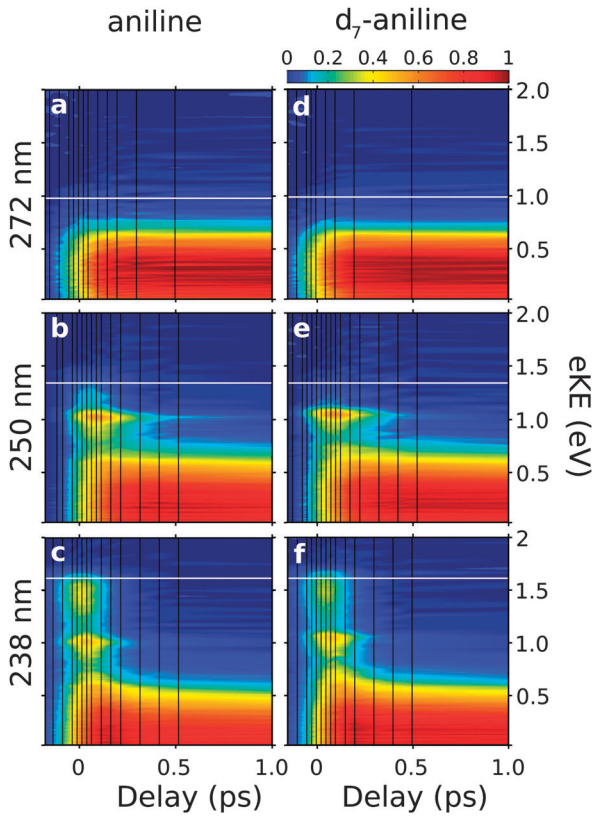

Fig. 2 Contour plots showing experimental time-resolved photoelectron spectra for aniline (a–c) and d_7-aniline (d–f), following excitation just below the $1^1\pi\sigma^*$ origin at 272 nm (4.56 eV), above the $1^1\pi\sigma^*$ origin at 250 nm (4.96 eV) and to the $2^1\pi\pi^*$ state at 238 nm (5.21 eV). Individual plots were normalised to their maximum photoelectron signals. The shading was smoothed using bilinear interpolation and the vertical black lines mark the pump–probe delays at which photoelectron spectra were recorded. Horizontal white lines mark the maximum eKE possible from 1 + 1′ ionisation, calculated using the central wavelengths of the pump and probe laser pulses and the adiabatic ionisation potential of 7.72 eV.[29]

all recent time-resolved photoelectron imaging experiments with aniline.[19–22] For each photoexcitation wavelength, the integrated areas of the photoelectron spectra have been scaled to the total integrated photoelectron signals at the corresponding pump–probe delays and plotted as a contour map. Notably, the time-resolved photoelectron spectra are very similar for aniline and d_7-aniline. The symmetric feature at low eKE, corresponding to ionisation from the $1^1\pi\pi^*$ state, is observed in all the contour maps and appears to have a lifetime >1 ps. The sharp feature around 1 eV, corresponding to ionisation from the $1^1\pi\sigma^*$ state, is observed in the 250 nm and 238 nm contour maps and appears to have a lifetime $\gtrsim 100$ fs. The asymmetric feature corresponding to ionisation from the $2^1\pi\pi^*$ state is observed in the 238 nm contour maps and appears to decay very rapidly, on a timescale <100 fs.

The observed dynamics were fit to eqn (1) and the lifetimes obtained are presented in Table 1. Only one lifetime was required to fit the 272 nm data sets, three lifetimes were required to fit the 250 nm data sets and four lifetimes were required to fit the 238 nm data sets.

Table 1 Summary of 1/*e* lifetimes extracted by fitting portions of the time-resolved photoelectron spectra of aniline and d_7-aniline to eqn (1). The errors quoted represent two standard deviations

	λ_{pump}/nm	τ_1/ps	τ_2/fs	τ_3/fs	τ_4/fs	$g(t)$/fs
aniline	272	600 ± 40				220 ± 120
	250	100 ± 8	570 ± 180	110 ± 20		190 ± 10
	238	90 ± 5	450[a]	130 ± 40	50 ± 10	230 ± 10
d_7-aniline	272	1300 ± 40				220 ± 110
	250	100 ± 6	480 ± 150	130 ± 20		180 ± 20
	238	82 ± 5	980 ± 510	130 ± 30	50 ± 10	220 ± 10

[a] Ref. 30.

The time-resolved photoelectron spectra were then fit to sums of the exponential decays listed in Table 1 convoluted with $g(t)$,

$$S(\mathrm{eKE},t) = \sum_i C_i(\mathrm{eKE})\mathrm{e}^{-t/\tau_i} \otimes g(t), \qquad (2)$$

where the coefficients C_i(eKE) represent the contribution of the ith decay at a given eKE. The spectra of the fit coefficients C_i(eKE) are plotted in Fig. 3. Positive values of C_i(eKE) represent exponential decay at timescale τ_i and negative values represent exponential growth at τ_i.

For all photoexcitation energies, the spectra associated with the τ_1 lifetime are centered around 0.2 eV with positive amplitude

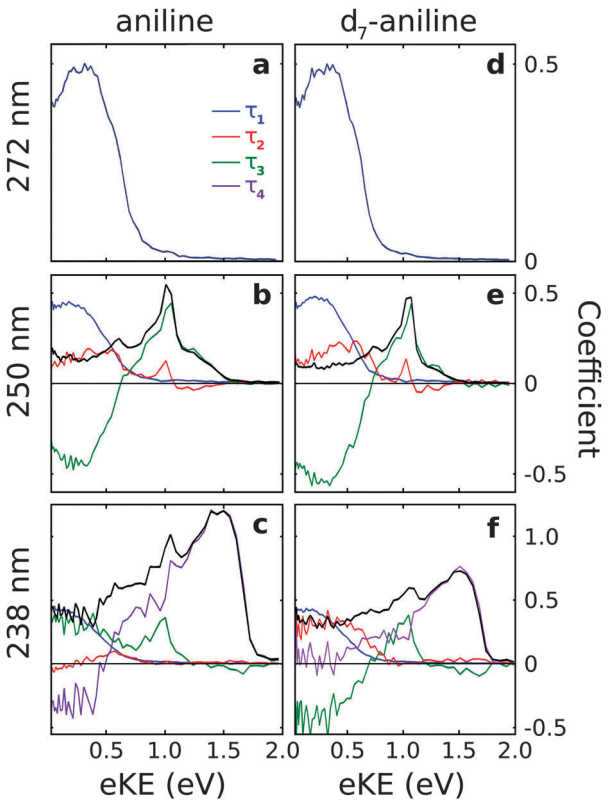

Fig. 3 Spectral components of C_i(eKE) extracted from the time-resolved photoelectron spectra (Fig. 2) using the decay times listed in Table 1 and eqn (2). The sum of C_i(eKE) (black lines) represents the photoelectron spectrum of the initially excited state.

components, indicating a decay of population from the $1^1\pi\pi^*$ state. Following photoexcitation at 250 nm, the spectra associated with the τ_2 lifetime extends from 0 eV to $\gtrsim$1 eV with positive amplitude components, indicating a decay of population on a timescale τ_2. In contrast, the spectra obtained for the τ_3 lifetime have sharp features around 1 eV with positive amplitude components and broad features centered around 0.2 eV with negative amplitude components. This suggests an evolution along the excited potential energy surface from the $1^1\pi\sigma^*$ state to the $1^1\pi\pi^*$ state with timescale τ_3.

Following photoexcitation of d_7-aniline at 238 nm, the spectra associated with the τ_2 and τ_3 lifetimes are similar to those observed at 250 nm, although the spectrum associated with the τ_2 timescale no longer has significant amplitude at 1 eV. The spectrum associated with the τ_4 timescale has a broad, asymmetric feature at high eKE with positive amplitude components, indicating a decay of population from the $2^1\pi\pi^*$ state with timescale τ_4. The absence of negative amplitude components prevents us identifying the fate of this population but it does not rule out the possibility of energy flow into $1^1\pi\sigma^*$ or $1^1\pi\pi^*$ states because the photoelectron spectra of these components overlap and the decay associated spectra are the sum of positive and negative amplitude components. In contrast, for aniline, the spectrum associated with the τ_2 timescale is much less intense than that for d_7-aniline, the spectrum associated with τ_3 only has positive amplitude components, both at low eKE and around 1 eV, and the spectrum associated with the τ_4 timescale has positive amplitude components at high eKE and negative amplitude components at low eKE, suggesting an evolution on the excited potential energy surface from the $2^1\pi\pi^*$ state into the $1^1\pi\pi^*$ state.

4 Discussion

To assist with the interpretation of the photoelectron spectra, we begin with a summary of the results of our recent theoretical investigation of the relaxation pathways following photoexcitation to the first few singlet excited states of aniline in Fig. 4.[23] On the $1^1\pi\pi^*$ potential energy surface (blue lines in Fig. 4), we found a prefulvene-like minimum energy conical intersection (MECI) connecting the $1^1\pi\pi^*$ state with the ground state in which the carbon-atom carrying the amino group is distorted out-of-plane. On the $1^1\pi\sigma^*$ potential energy surface (green lines in Fig. 4), we found a MECI connecting the $1^1\pi\sigma^*$ state and the $1^1\pi\pi^*$ state close to the local minimum on the $1^1\pi\sigma^*$ surface, suggesting that population on the $1^1\pi\sigma^*$ surface could relax through this MECI to the $1^1\pi\pi^*$ state and to the dissociative component of the $1^1\pi\sigma^*$ state. On the $2^1\pi\pi^*$ state (orange lines in Fig. 4) we found evidence for a barrierless pathway from the Franck–Condon geometry to the ground state through a three-state conical intersection involving the $2^1\pi\pi^*$, $1^1\pi\pi^*$ and $1^1\pi\sigma^*$ states.

The experiments presented in this paper confirm our earlier observation that four time constants are required to characterise

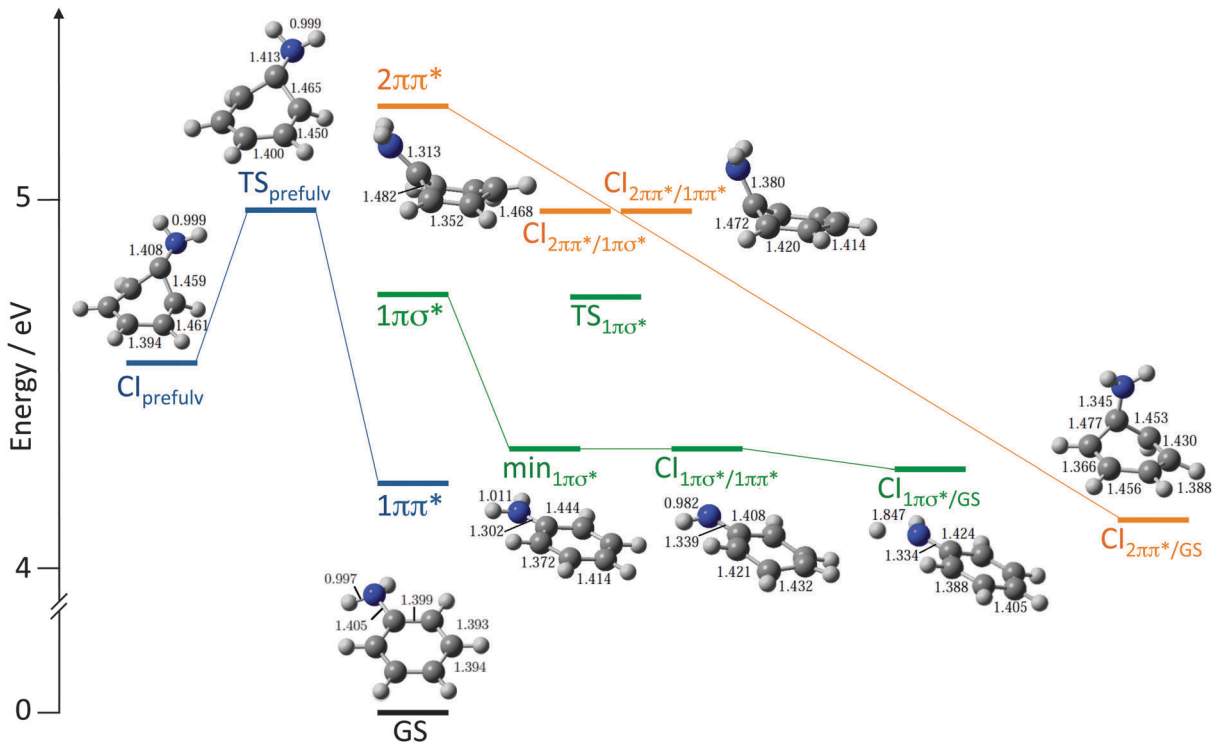

Fig. 4 Schematic diagram illustrating key features on the potential energy landscape and relaxation pathways following photoexcitation to the first few singlet excited states of aniline.[23] The vertical excitation energies of the $1^1\pi\pi^*$, $1^1\pi\sigma^*$ and $2^1\pi\pi^*$ levels, calculated at the XMCQDPT2 level of theory, are plotted vertically above the minimum energy of the ground electronic state (GS). XMCQDPT2 energies of key transition states (TS), minima (min) and conical intersections (CI) on the $1^1\pi\pi^*$ (blue), $1^1\pi\sigma^*$ (green) and $2^1\pi\pi^*$ surfaces (orange) are presented together with their corresponding CASSCF geometries.

the photochemistry of aniline following photoexcitation in the range 272–238 nm,[19,20] which is consistent with the existence of at least four relaxation pathways.

The longest time constant τ_1 corresponds to the decay of population from the $1^1\pi\pi^*$ state. It has been suggested that following excitation close to the $1^1\pi\sigma^*$ origin, population on the $1^1\pi\pi^*$ state may tunnel through the barrier formed by the crossing between the $1^1\pi\pi^*$ and $1^1\pi\sigma^*$ states onto the dissociative part of the $1^1\pi\sigma^*$ surface,[16,18,21] as has been observed in phenol.[12,31–34] Tunnelling is sensitive to the mass of the particle involved and therefore the time constant for a relaxation mechanism involving tunnelling of one of the H-atoms of the amino group would be expected to be significantly longer for d_7-aniline than aniline. However, τ_1 is only a factor of two longer for d_7-aniline (Table 1), which is not enough to be attributed to quantum mechanical tunnelling although it can be accounted for by differences in the vibration frequencies between aniline and d_7-aniline. Thus, we do not find any evidence to support the suggestion that tunnelling occurs through the barrier formed by the crossing between the $1^1\pi\pi^*$ and $1^1\pi\sigma^*$ states in aniline, which is surprising given that such tunnelling has been observed in isoelectronic phenol. We therefore interpret τ_1 as the lifetime for intramolecular vibrational redistribution (IVR), intersystem crossing (ISC)[11] or fluorescence[10] following excitation close to the $1^1\pi\sigma^*$ origin.

Following excitation with wavelengths $\lesssim$250 nm, the prefulvene MECI connecting the $1^1\pi\pi^*$ state with the ground state is accessible (Fig. 4). Thus, following excitation above the barrier between the Franck–Condon region and this MECI, it is likely that τ_1 corresponds to the lifetime for IC through the prefulvene MECI. The decrease in lifetime with increase in photoexcitation energy is consistent with the presence of a barrier.

Curiously, whereas we only need one time constant to fit the aniline and d_7-aniline time-resolved photoelectron spectra recorded following photoexcitation at 272 nm and photoionisation at 300 nm (Fig. 3a and d), Thompson and coworkers found that an additional time constant of 640 fs was required to fit the time-resolved photoelectron spectra of aniline they recorded following excitation at 273 nm and photoionisation at 305 nm.[21] They attributed the additional time constant to IVR on the $1^1\pi\pi^*$ surface. We cannot explain the difference between the two experiments as it seems unlikely that an IVR promoting mode is accessible in the $1^1\pi\pi^*$ state at 273 nm photoexcitation in aniline but not at 272 nm in either aniline or d_7-aniline.

The τ_3 time constant corresponds to a decay of population from the $1^1\pi\sigma^*$ state and an increase of population in the $1^1\pi\pi^*$ state, following photoexcitation at 250 nm (Fig. 3b and e). This supports our earlier proposal that following photoexcitation above the $1^1\pi\sigma^*$ origin, the $1^1\pi\sigma^*$ state is excited directly and relaxes through the MECI connecting the $1^1\pi\sigma^*$ and $1^1\pi\pi^*$ states close to the local minimum on the $1^1\pi\sigma^*$ surface (Fig. 4).[19,20,23] The MECI funnels population to the $1^1\pi\pi^*$ surface and also to the dissociative component of the $1^1\pi\sigma^*$ state, which has been monitored directly in femtosecond pump–probe velocity map imaging experiments.[18] We do not observe any population flow from the $1^1\pi\pi^*$ state to the $1^1\pi\sigma^*$ state, so it seems unlikely that direct excitation of the $1^1\pi\pi^*$ state is followed by relaxation through the MECI to the dissociative component of the $1^1\pi\sigma^*$ state, as suggested by King and coworkers[16] and Roberts and coworkers,[18] although we cannot rule out the possibility that there is a small contribution from such a relaxation mechanism that is not revealed by our fitting procedure. We note that a very recent study of the dynamics of aniline reported by Thompson and coworkers supports our conclusions.[22]

In aniline, the τ_4 time constant corresponds to a rapid ($<$50 fs) flow of population from the $2^1\pi\pi^*$ state to the $1^1\pi\pi^*$ state and there is a decay of population from both the $1^1\pi\sigma^*$ and $1^1\pi\pi^*$ states with a τ_3 time constant (Fig. 3c). In d_7-aniline, the τ_4 time constant corresponds to a rapid ($<$50 fs) decay of population from the $2^1\pi\pi^*$ state out of the observation window of our experiment, and a flow of population from the $1^1\pi\sigma^*$ state to the $1^1\pi\pi^*$ state with a τ_3 time constant (Fig. 3f). The rapid flow of population from the $2^1\pi\pi^*$ state following excitation at 238 nm is consistent with our proposal that population decays along a barrierless path to the ground-state, through a CI between the $2^1\pi\pi^*$ state and the ground-state.[19,20] It is also worth noting that similar ring-puckering relaxation pathways have been observed in other simple aromatic molecules such as pyrrole,[35] and the purine DNA bases adenine[36,37] and guanine.[38] Moreover, the boat conformation of the phenyl ring at the CI between the $2^1\pi\pi^*$ state and the ground-state (Fig. 4) resembles the Dewar form of benzene, which is known to be populated following photoexcitation of the $2^1\pi\pi^*$ state of benzene.[39,40] However, our observation of population in the $1^1\pi\sigma^*$ and $1^1\pi\pi^*$ states at short times is consistent with passage through a three-state CI involving the $2^1\pi\pi^*$, $1^1\pi\pi^*$ and $1^1\pi\sigma^*$ states. It is worth noting that it is unlikely that there is significant direct population of $1^1\pi\sigma^*$ and $1^1\pi\pi^*$ states at 238 nm. Thus, our new experiments support our earlier proposal that following excitation of the $2^1\pi\pi^*$ state the majority of the excited state population is transferred directly back to the ground state,[19,20] but it seems likely that some population is also transferred to the $1^1\pi\pi^*$ and $1^1\pi\sigma^*$ states at a three-state CI involving the $2^1\pi\pi^*$, $1^1\pi\pi^*$ and $1^1\pi\sigma^*$ states. From the $1^1\pi\sigma^*$ and $1^1\pi\pi^*$ states, the molecule can then relax directly to the Franck–Condon geometry from where it can then relax through the prefulvene MECI connecting the $1^1\pi\pi^*$ state with the ground state (τ_1) or through the MECI connecting the $1^1\pi\sigma^*$ and $1^1\pi\pi^*$ states close to the local minimum on the $1^1\pi\sigma^*$ (τ_3).

The τ_2 time-constant has been another subject of debate. Its broad decay associated spectrum originally led us to assign it to dynamics on the $1^1\pi\sigma^*$ surface, possibly trapping,[19,20] and Thompson and coworkers to assign it to IVR on the $1^1\pi\pi^*$ surface.[21] The values of τ_2 (Table 1) are similar to timescales that have been attributed to ultrafast IVR processes on the $1^1\pi\pi^*$ surfaces of phenol, catechol, resorcinol, and hydroquinone.[41] However, we do not observe any dynamics with a τ_2 time-constant following excitation below the $1^1\pi\sigma^*$ origin, so we believe this time-constant must correspond to dynamics on the $1^1\pi\sigma^*$ surface. Interestingly, Domcke and coworkers also found two time constants associated with the $1^1\pi\sigma^*$ surface of pyrrole

which, like aniline, has a quasi-bound well close to the Franck–Condon region and a dissociative potential curve along the N–H stretching coordinate.[42] Their wave packet calculations revealed time constants of ~10 fs and several hundreds of femtoseconds, corresponding to direct decay over the barrier and tunnelling through the barrier, respectively. However, τ_2 has similar values for aniline and d_7-aniline following photoexcitation at 250 nm (Table 1) and similar values over a range of excitation energies (Table 1 and ref. 20), which rules out tunnelling. Thus, we still conclude that there are two time constants associated with dynamics on the $1^1\pi\sigma^*$ surface in aniline: τ_3 associated with flow of population through the CI between the $1^1\pi\sigma^*$ and $1^1\pi\pi^*$ states and τ_2 associated with motion on the $1^1\pi\sigma^*$ surface, although we concede that IVR may be a better description of the dynamics with time constant τ_2. Quantum dynamics calculations may help gain further insight into the dynamics on the $1^1\pi\sigma^*$ surface.

5 Conclusions

New femtosecond time-resolved photoelectron spectroscopy experiments following photoexcitation of aniline and d_7-aniline from below the $1^1\pi\sigma^*$ origin to the $2^1\pi\pi^*$ state have resolved a number of unanswered questions surrounding various electronic relaxation mechanisms.

(1) We did not find evidence to support the suggestion that following excitation close to the $1^1\pi\sigma^*$ origin, tunnelling occurs through the barrier on the $1^1\pi\sigma^*$ potential surface.[16,18,21] We attribute the dynamics following excitation below the $1^1\pi\sigma^*$ origin in aniline and d_7-aniline to IVR on the $1^1\pi\pi^*$ surface, ISC or fluorescence. Following photoexcitation above the barrier between the Franck–Condon geometry and the prefulvene MECI connecting the $1^1\pi\pi^*$ state with the ground state, we attribute the dynamics on the $1^1\pi\pi^*$ surface to relaxation through the prefulvene MECI.

(2) We observe clear evidence to support the conclusions of our earlier experiments that following photoexcitation above the $1^1\pi\sigma^*$ origin, the $1^1\pi\sigma^*$ state is excited directly and relaxes through the MECI connecting the $1^1\pi\sigma^*$ and $1^1\pi\pi^*$ states close to the local minimum on the $1^1\pi\sigma^*$ surface.[19,20,23] Although we do not observe population flow from the $1^1\pi\pi^*$ state to the $1^1\pi\sigma^*$ state, it is possible that there could be a small contribution from direct excitation of the $1^1\pi\pi^*$ state followed by relaxation through the MECI to the dissociative component of the $1^1\pi\sigma^*$ state. We conclude that there is also a second time constant associated with dynamics on the $1^1\pi\sigma^*$ surface.

(3) We find compelling evidence to support our proposal that non-radiative decay from the $2^1\pi\pi^*$ state involves a barrierless pathway from the Franck–Condon region to a CI between the $2^1\pi\pi^*$ state and the ground-state that passes through a three-state conical intersection involving the $2^1\pi\pi^*$, $1^1\pi\sigma^*$ and $1^1\pi\pi^*$ states.[23]

In summary, this work demonstrates that tunnelling does not play a role in the electronic relaxation dynamics of aniline following photoexcitation in the range 272–238 nm, which is surprising given that tunnelling has been found to play an important role in the electronic relaxation of the isoelectronic molecule phenol and in pyrrole. To the best of our knowledge, this work also provides the first experimental signature of a 3-state conical intersection. Detailed gas-phase experiments such as this, combined with the results of detailed theoretical studies, are essential in forming a good starting point for understanding the relaxation mechanisms of these biologically relevant chromophores in realistic environments.

Acknowledgements

This work was supported by the EPSRC, European Marie Curie Initial Training Network Grant No. GA-ITN-214962-FASTQUAST, Conseil Regional de Bourgogne and the Spanish Ministry of Economy and Competitiveness (MINECO) through grant CTQ2012-37404-C02-01. The authors are grateful to David Townsend (Herriot-Watt) for valuable discussions.

References

1 M. N. R. Ashfold, G. A. King, D. Murdock, M. G. D. Nix, T. A. A. Oliver and A. G. Sage, *Phys. Chem. Chem. Phys.*, 2010, **12**, 1218–1238.
2 G. M. Roberts and V. G. Stavros, in *The role of * states in the photochemistry of heteroaromatic biomolecules and their subunits: insights from gas-phase femtosecond spectroscopy*, ed. R. de Nalda and L. Banares, Springer-Verlag, Berlin, 2014, vol. 107, pp. 119–143.
3 C. T. Middleton, K. de La Harpe, C. Su, Y. K. Law, C. E. Crespo-Hernández and B. Kohler, *Annu. Rev. Phys. Chem.*, 2009, **60**, 217–239.
4 T. Gustavsson, R. Improta and D. Markovitsi, *J. Phys. Chem. Lett.*, 2010, **1**, 2025–2030.
5 C. C.-W. Cheng, C. Ma, C. T.-L. Chan, K. Y.-F. Ho and W.-M. Kwok, *Photochem. Photobiol. Sci.*, 2013, **12**, 1351–1365.
6 X. Song, M. Yang, E. R. Davidson and J. P. Reilly, *J. Chem. Phys.*, 1993, **99**, 3224.
7 T. Ebata, C. Minejima and N. Mikami, *J. Phys. Chem. A*, 2002, **106**, 11070–11074.
8 E. R. T. Kerstel, M. Becucci, G. Pietraperzia and E. Castellucci, *Chem. Phys.*, 1995, **199**, 263–273.
9 K. Kimura, H. Tsubomura and S. Nagakura, *Bull. Chem. Soc. Jpn.*, 1964, **37**, 1336–1346.
10 R. Scheps, D. Florida and S. A. Rice, *J. Chem. Phys.*, 1974, **61**, 1730–1747.
11 B. Kim, C. P. Schick and P. M. Weber, *J. Chem. Phys.*, 1995, **103**, 6903–6913.
12 A. L. Sobolewski, W. Domcke, C. Dedonder-Lardeux and C. Jouvet, *Phys. Chem. Chem. Phys.*, 2002, **4**, 1093–1100.
13 H. Reisler and A. I. Krylov, *Int. Rev. Phys. Chem.*, 2009, **28**, 267–308.
14 F. Wang, S. P. Neville, R. Wang and G. A. Worth, *J. Phys. Chem. A*, 2013, **117**, 7298–7307.
15 B. N. Rajasekhar, A. Veeraiah, K. Sunanda and B. N. Jagatap, *J. Chem. Phys.*, 2013, **139**, 064303.

16 G. A. King, T. A. A. Oliver and M. N. R. Ashfold, *J. Chem. Phys.*, 2010, **132**, 214307.
17 R. Montero, Á. P. Conde, V. Ovejas, R. Martínez, F. Castaño and A. Longarte, *J. Chem. Phys.*, 2011, **135**, 054308.
18 G. M. Roberts, C. A. Williams, J. D. Young, S. Ullrich, M. J. Paterson and V. G. Stavros, *J. Am. Chem. Soc.*, 2012, **134**, 12578–12589.
19 R. Spesyvtsev, O. M. Kirkby, M. Vacher and H. H. Fielding, *Phys. Chem. Chem. Phys.*, 2012, **14**, 9942–9947.
20 R. Spesyvtsev, O. M. Kirkby and H. H. Fielding, *Faraday Discuss.*, 2012, **157**, 165–179.
21 J. O. F. Thompson, R. A. Livingstone and D. Townsend, *J. Chem. Phys.*, 2013, **139**, 034316.
22 J. O. F. Thompson, L. Saalbach, S. W. Crane, M. J. Paterson and D. Townsend, *J. Chem. Phys.*, 2015, **142**, 114309.
23 M. Sala, O. M. Kirkby, S. Guérin and H. H. Fielding, *Phys. Chem. Chem. Phys.*, 2014, **16**, 3122–3133.
24 D. S. N. Parker, R. S. Minns, T. J. Penfold, G. A. Worth and H. H. Fielding, *Chem. Phys. Lett.*, 2009, **469**, 43–47.
25 R. S. Minns, D. S. N. Parker, T. J. Penfold, G. A. Worth and H. H. Fielding, *Phys. Chem. Chem. Phys.*, 2010, **12**, 15607–15615.
26 A. D. G. Nunn, R. S. Minns, R. Spesyvtsev, M. J. Bearpark, M. A. Robb and H. H. Fielding, *Phys. Chem. Chem. Phys.*, 2010, **12**, 15751–15759.
27 G. A. Garcia, L. Nahon and I. Powis, *Rev. Sci. Instrum.*, 2004, **75**, 4989–4996.
28 J. E. Hansen and W. Persson, *Phys. Scr.*, 1987, **36**, 602–643.
29 M. A. Smith, J. W. Hager and S. C. Wallace, *J. Chem. Phys.*, 1984, **80**, 3097–3105.
30 This lifetime was difficult to fit due to its small amplitude (Fig. 3c) but excluding it resulted in a poor fit. The value of 450 fs was selected to give a reasonable fit to the experimental data.
31 G. A. Pino, A. N. Oldani, E. Marceca, M. Fujii, S. I. Ishiuchi, M. Miyazaki, M. Broquier, C. Dedonder and C. Jouvet, *J. Chem. Phys.*, 2010, **133**, 124313.
32 R. N. Dixon, T. A. A. Oliver and M. N. R. Ashfold, *J. Chem. Phys.*, 2011, **134**, 194303.
33 H. An and K. K. Baeck, *J. Phys. Chem. A*, 2011, **115**, 13309–13315.
34 G. M. Roberts, A. S. Chatterley, J. D. Young and V. G. Stavros, *J. Phys. Chem. Lett.*, 2012, **3**, 348–352.
35 M. Barbatti, M. Vazdar, A. J. A. Aquino, M. Eckert-Maksić and H. Lischka, *J. Chem. Phys.*, 2006, **125**, 164323.
36 L. Blancafort, *J. Am. Chem. Soc.*, 2006, **128**, 210–219.
37 S. Perun, A. L. Sobolewski and W. Domcke, *J. Am. Chem. Soc.*, 2005, **127**, 6257–6265.
38 L. Serrano-Andrés, M. Merchán and A. C. Borin, *J. Am. Chem. Soc.*, 2008, **130**, 2473–2484.
39 H. R. Ward and J. S. Wishnok, *J. Am. Chem. Soc.*, 1968, **90**, 5353–5357.
40 A. L. Sobolewski, *J. Chem. Phys.*, 1990, **93**, 6433–6439.
41 R. A. Livingstone, J. O. F. Thompson, M. Iljina, R. J. Donaldson, B. J. Sussman, M. J. Paterson and D. Townsend, *J. Chem. Phys.*, 2012, **137**, 184304.
42 V. Vallet, Z. Lan, S. Mahapatra, A. L. Sobolewski and W. Domcke, *J. Chem. Phys.*, 2005, **123**, 144307.